University of Texas at El Paso
ScholarWorks@UTEP

Open Access Theses & Dissertations

2020-01-01

Shallow Seismic Modeling Of The Hydrothermal Plumbing System Beneath Old Faithful Geyser In The Upper Geyser Basin Of Yellowstone National Park

Jordan Rigdon Caylor
University of Texas at El Paso

Follow this and additional works at: https://scholarworks.utep.edu/open_etd

 Part of the Geology Commons, Geophysics and Seismology Commons, and the Hydrology Commons

Recommended Citation

Caylor, Jordan Rigdon, "Shallow Seismic Modeling Of The Hydrothermal Plumbing System Beneath Old Faithful Geyser In The Upper Geyser Basin Of Yellowstone National Park" (2020). *Open Access Theses & Dissertations*. 2945.
https://scholarworks.utep.edu/open_etd/2945

This is brought to you for free and open access by ScholarWorks@UTEP. It has been accepted for inclusion in Open Access Theses & Dissertations by an authorized administrator of ScholarWorks@UTEP. For more information, please contact lweber@utep.edu.

SHALLOW SEISMIC MODELING OF THE HYDROTHERMAL PLUMBING SYSTEM BENEATH OLD FAITHFUL GEYSER IN THE UPPER GEYSER BASIN OF YELLOWSTONE NATIONAL PARK

JORDAN RIGDON CAYLOR

Master's Program in Geophysics

APPROVED:

Marianne Karplus, Ph.D., Chair

Julien Chaput, Ph.D.

Jamie Farrell, Ph.D.

Stephen L. Crites, Jr., Ph.D.
Dean of the Graduate School

Copyright ©

by

Jordan Rigdon Caylor

2020

SHALLOW SEISMIC MODELING OF THE HYDROTHERMAL PLUMBING SYSTEM BENEATH OLD FAITHFUL GEYSER IN THE UPPER GEYSER BASIN OF YELLOWSTONE NATIONAL PARK

by

Jordan Rigdon Caylor, B.S.

THESIS

Presented to the Faculty of the Graduate School of

The University of Texas at El Paso

in Partial Fulfillment

of the Requirements

for the Degree of

MASTER OF SCIENCE

Department of Geological Sciences

THE UNIVERSITY OF TEXAS AT EL PASO

May 2020

Acknowledgements

I would like to acknowledge all the people at the University of Texas at El Paso, the University of Utah and Yellowstone National Park who contributed to this work. Without the help of my committee, professors, and colleagues I don't think I could have written this thesis. I especially would like to thank those who collected this data in the field. Without the field work none of this would be possible.

Abstract

In November 2016, a 2-D and 3-D seismic survey was performed around Old Faithful Geyser in the southeastern portion of the Upper Geyser Basin in Yellowstone National Park. The survey consisted of 521 3-component seismic receiver locations including 39 receivers on a ~1km NE-SW trending line crossing Old Faithful Geyser. A 5.4kg sledgehammer striking a metal plate was our source with a dominant frequency of ~40Hz. Our 2-D line crosses Old Faithful in a NE-SW direction with station spacing at 25-30m with ~100m spacing on either side of Old Faithful and a total length of 1024m. Our 3-D seismic grid is an array of 521 receivers and 343 shots covering an area of ~4km^2 with an average station spacing of 22m. We create tomographic profiles and velocity models in 2-D to visualize the subsurface structure surrounding Old Faithful in an attempt to visualize the main reservoir body of OFG. We recover a low velocity anomaly SW of Old Faithful which may be a reservoir feeding into the plumbing system. Our receivers were deployed at any given location for at least 1 or 2 days making this data set viable for passive source modeling as well. We explore the effectiveness of using the H/V ratio to study the subsurface at Old Faithful. This study provides new insight into the subsurface structure of Old Faithful Geyser and the southern portion of The Upper Geyser Basin.

Table of Contents

List of Figures

Seismic Modeling of Old Faithful Geyser

Introduction

The Yellowstone hotspot is the volcanic hotspot responsible for large scale volcanism that created the 0.63 Ma Yellowstone Caldera and hydrothermal features observed in northwestern Wyoming, USA (Figure 1) (Huang et al., 2015; Farrell, et al., 2014; Smith et al., 2009). The mantle plume generates melts at depths of ~60km which rise buoyantly and eventually heat hydrothermal fluids that rise through steeply dipping faults at ~5km to shallow reservoirs (Foley et al., 2014; Huang et al., 2015). Geysers are formed when the unique combination of subsurface cracks and hydrothermal fluids create a system to expel groundwater at the surface (Ardid et al., 2019). The Yellowstone hotspot has created the largest concentration of geysers on Earth. Within Yellowstone National Park, the Upper Geyser Basin (UGB) hosts the park's highest concentration of hydrothermal features as well as one of the largest subsurface hydrothermal systems (Foley et al., 2014). This study is being conducted to better understand the hydrothermal plumbing system beneath Old Faithful Geyser (OFG) and constrain a proposed relatively large reservoir body SW of OFG (Wu et al., 2017) using a shallow active source seismic refraction study. Old Faithful is located adjacent to historic park infrastructure, and part of the goal of this project is to identify locations with hydrothermal activity in the subsurface to inform future park building projects and renovations. Furthermore, we will be exploring what information about the subsurface we may gain by calculating H/V spectral ratios (i.e., the ratio between the Fourier amplitude spectra of the horizontal and vertical component seismic recordings) in an active hydrothermal field.

The sight of an OFG eruption has attracted visitors for almost 150 years. Although the time intervals between eruptions are regular on a day to day timescale, the OFG system is

delicate and has changed over time (Foley et al., 2014). The time interval between eruptions can change after large earthquakes and the time between eruptions has increased by ~50 minutes since it was first recorded (Foley et al., 2014, Hurwitz & Lowenstern., 2014). Therefore, it is important to understand the elements of the system which are critical to eruptions. By constraining the proposed reservoir SW of OFG we may better understand how the system works (Wu et al., 2017).

Geologic Background

OFG is situated in the Firehole River Valley where the geology around OFG is predominantly glacial deposits, siliceous sinter, and igneous flows (Foley et al., 2014; Fenner, 1936; Honda & Muffler 1970; Keith et al., 1978; Lynne et al., 2018; Muffler et al., 1982). In 1929 the Carnegie Institute drilled a research hole, C-1, ~400 m southwest of Old Faithful providing insight into the subsurface lithology (Fenner, 1936). The location of the C-1 hole can be seen in figure 2. The drill hole went through sinter until reaching a mixture of rhyolitic pebbles at 2.1m which increased in percent of rhyolite until 12.2m (Fenner, 1936). At 12.2m the hole penetrated gravel cemented with opaline silica & secondary quartz (Fenner, 1936). From 12.2m to 18.9m the well went through hydrothermally altered sediments until reaching dacitic bedrock with interbedded obsidian at 67.1m (Fenner, 1936). The well saw no major change in lithology from 67.1m to 123.7m and was filled with cement at 123.7m (Fenner, 1936). The sedimentary layers of sandstone and conglomerate penetrated were likely deposited as outwash from the early waning stages of the Pinedale Glaciation (Honda & Muffler 1970). The C-1 drill hole report gave us an initial idea of the lithologies present in the subsurface which were used to create starting velocity models.

The surficial geology around Old Faithful is predominantly sinter with rhyolite exposed northeast of the geyser across the Firehole River with glacial deposits to the south and west (Muffler et al., 1982). Altered glacial deposits and igneous flows create zones of saturated media in the subsurface. The surficial geology and our 2-D line are shown in figure 2a. Understanding the geologic system at OFG allows for more detailed assessment of areas in the subsurface that are critical to remaining undisturbed by human activity (Foley et al., 2014).

Hydrogeologic Background

The hydrothermal system feeding the UGB is heated by the rhyolitic upper crustal magma reservoir at ~5-15km (Foley et al., 2014; Huang et al., 2015; Farrell et al., 2014). Chemical thermometry studies have found that the waters erupted at Old Faithful rise from ~5km in the subsurface from a deep reservoir (Foley et al., 2014). Fracture networks created from ongoing seismic activity and hydrothermal alteration of the lithology in the area have created plumbing conduits in which ground water is brought to the surface from deeper reservoirs (Foley et al., 2014). Hydrothermal fluids follow steep faults and cracks to shallower reservoirs at ~170-210m (Foley et al., 2014). From this recharge zone the fluids migrate through a ~35m vertical conduit to an inferred bubble trap then migrate laterally ~20m before rising vertically to the surface (Wu et al. 2017; Vandemeulebrouck et al. 2013). Two of the current models of Old Faithful Geyser's plumbing system can be seen in figure 3 (Wu et al., 2017; Wu et al., 2019; Vandemeulebrouck et al., 2013). A combination of deep and near-surface hydrothermal activity is responsible for the incredible geyser field in the UGB. Understanding the structure of the conduit that feeds Old Faithful is important because it will show us which areas in the subsurface have active geothermal activity.

Working in a hydrothermal field presents challenges to interpreting seismic data, in part due to the seismic background 'noise' related to the fluid movements in the subsurface. The constant activity of bubbling and fluid migration introduces high-amplitude background seismic noise to the active source data which occur around ~5-20Hz (Kedar et al., 1998; Wu et al., 2017; Vandemeulebrouck et al., 2013). Our source has a dominant frequency of ~40Hz; therefore, we use a bandpass filter to remove some of the noise from the data.

Relevant Geophysical Studies

Old Faithful plumbing structure investigation via source localization. Utilizing a dense seismic network of 96 receivers, beamforming techniques were applied to track bubble collapse in the Old Faithful Geyser plumbing system (Vandemeulebrouck et al., 2013). This study reported a cavity southwest of Old Faithful's main vent and ~15m below the surface (Vandemeulebrouck et al., 2013). Collapsing bubbles in Old Faithful Geyser's plumbing system produces seismic signals at frequencies between ~5-10Hz (Vandemeulebrouck et al., 2013). Furthermore, as the bubbles rise to the near surface (~10m below the surface) there is an increase in amplitude in the resulting seismic signal (Vandemeulebrouck et al., 2013).

Cross Correlation Function Study of Old Faithful Geyser. Wu et al. (2017) used a dense three-component array of nodal seismometers to extract Rayleigh wave seismic signals between 1 and 10 Hz using seismic waves excited by active hydrothermal features in order to examine the subsurface structure of Old Faithful Geyser (Wu et al., 2017). The seismic array utilized in that study consisted of 133 3-component 5Hz nodal seismometers that were deployed over the course of 12 days (11/02/2015-11/14/2015) with an average spacing of ~50 m with a radial coverage of about 1 km (Wu et al., 2017). Wu et al. (2017) performed spectral whitening and then calculated cross-correlation functions between all station pairs (Wu et al., 2017). They observed coherent

signals in the cross-correlation functions between a station on Geyser Hill and all other stations across the array and used those functions to measure Rayleigh wave phase velocities by applying standard frequency-time analysis (Wu et al., 2017). A Rayleigh wave phase velocity increase of ~40% in the northeast was observed for frequencies of 3.33 Hz and interpreted as the higher velocity rhyolitic flows compared to the lower velocity glacial sediments to the southwest (Wu et al., 2017). Another major result relevant to this study is that Wu et al. (2017) observed a low velocity zone starting 100m to the southwest of Old Faithful at a depth of about 22m with an estimated diameter of ~200 m (Wu et al., 2017). The Rayleigh wave phase velocities were observed to be reduced by ~70% in the low velocity zone relative to the surrounding glacial deposits. The low velocity zone is interpreted as a fractured and porous media which acts to recharge the waters which erupt from Old Faithful. It is believed that this deeper fractured zone allows water to fill into a shallower reservoir through vertical and horizontal conduits connecting reservoirs (Wu et al, 2017; Vandemeulebrouck et al, 2013). The model proposed by Wu et al. (2017) is compared with our models derived from P-wave seismic refraction.

Seismic and resistivity study of the Obsidian Pool Thermal Area (OPTA). This 2016 survey of the OPTA imaged shallow hydrothermal degassing (Pasquet et al., 2016). The authors used Poisson's ratio (calculated from a combination of seismic refraction and surface-wave surveys) and electrical resistivity to characterize zones of anomalous velocity relating to fluid saturation in order to study degassing (Pasquet et al., 2016). This study found that larger values of Poisson's ratio correlate well to zones of high saturation in hydrothermal fields (Pasquet et al., 2016). While this study is not directly related to the Upper Geyser Basin, they also used a hammer seismic refraction survey to study a geothermal area.

Hydrogeology, geochemistry, and geomorphology study of the Upper Geyser Basin

Blackwood et al. (2018) investigated the origin, function, and evolution of the Old Faithful Geyser system (Blackwood et al., 2018). This study suggests that the dome-like structure of the shallowest reservoir may be due to condensation corrosion (Blackwood et al., 2018; Wu et al., 2017; Vandemeulebrouck et al., 2013). Condensation corrosion widens vents and conduits which may be responsible for the increased eruption interval times since the 1950's (Blackwood et al., 2018). Blackwood et al., 2018 also theorized that geysers situated near one another may share common reservoirs to extinct and extant geysers (Blackwood et al., 2018).

Objectives

The aim of this study is to determine the shallow structure of a proposed large reservoir, described by Wu et al. (2017), related to the hydrothermal plumbing system of OFG. Furthermore, we test how effective the H/V ratio is when applied to studying the shallow subsurface of OFG. Understanding the shallow extent of this proposed reservoir structure is useful in preserving and understanding the OFG hydrothermal systems as well as protecting nearby human infrastructure.

Data & Methods

From 11/7/2016 to 11/16/2016, dense 2-D and 3-D seismic arrays were deployed around a ~4km^2 area around OFG (figure 2). During those 10 days, we collected active source seismic data on 8 of those days with ~160 receivers and ~55 shots per day. Our 2-D line was collected on 11/08/2016 consisting of 39 receivers and 39 shot locations with a length of ~1020m crossing the OFG orifice in a NE-SW orientation (figure 2). The 2-D line has a station spacing of ~20-30m and ~100m gap with no stations on either side of the geyser. Our full 3-D array consisted of 521 receiver locations and 343 shot locations (figure 2). Multiple (5-7) strikes from a 5.4kg sledgehammer at each shot location allows us to stack our shots in the same location to amplify the signal and increase the signal to noise ratio. Stacked shot records from three different locations along our 2-D line are shown in figure 4. To study the structure of the reservoir body

SW of OFG we invert manually picked first arriving P-waves to create P-wave velocity (V_p) profiles using the Tomo2D software described by Korenaga et al. (2000). Tomographic V_p models are a practical method for this study, providing greater shallow resolution of the reservoir body over a broader area than previous studies.

Data Preparation & Picking

Tomographic profiles generated from inversions of first arriving waves allow us to model changes in the V_p velocity in the subsurface which likely relates to saturation, hydrothermal reservoirs, and hydrothermal alteration. We used Python scripts to convert the data from SAC to SEG-Y format and to stack the shots done in the same location. Next, we processed the data by performing trace muting and bandpass filtering to isolate the dominant source frequency. We applied an Ormsby minimum phase bandpass filter, with corner frequencies of 5-25-50-100Hz, to increase the signal and damp the low frequency signals of the OFG bubble collapse. First arriving P-waves were then picked manually. We observe these picks in the Z-component. First arriving waves can be picked further from the source in the northeastern side of our line on average and have a higher velocity (figure 5). This is likely due to the lithological change from glacial deposits in the SW to rhyolites in the NE (figures 2 & 3) (Muffler et al., 1982; Wu et al., 2017). The maximum offset we pick first arrivals is ~300 meters. On average we pick arrivals from the shot to 12 stations, and at maximum we track the arrival to 22 stations. In total we have 477 picks for the 39 shots. Furthermore, we do not observe many rays crossing the gap from one side of Old Faithful Geyser to the other (figure 5).

Tomographic Modeling

First arriving picks are input into Tomo2D tomographic inversion software (Korenaga et al., 2000) along with an initial model which influences the inversion. Initial models were created

based on previous research and geologic models (figure 6a & 6b) (Fenner 1936; Muffler et al., 1982; Wu et al., 2017)**.** Final models were highly sensitive to the initial model inputs and would often not converge to a final model. The outcomes of bad initial models were either unrealistic or physically impossible containing velocity nodes with non-positive values. We present two models which were most successful from the inversion having relatively low RMS error, stability, and relatively good ray coverage.

Tomo2D allows the user to generate sheared velocity meshes that can be finely edited with anomalous velocity zones and options for statistical analysis on the velocity meshes (Korenaga et al., 2000). Velocity meshes are used to calculate forward travel times followed by travel time inversions (Korenaga et al., 2000). The mesh spacings we used are defined in the horizontal direction as the distance between stations. We used a hanging mesh from this surface with 1m spacing between mesh nodes in the vertical direction to 100m below the surface. The velocity mesh used for this study can be seen in figure 7. Bilinear interpolation is used to determine the velocity of a point between nodes in the velocity mesh (Korenaga et al., 2000). Inversions are done using a damped and smoothed least squares regression algorithm (Korenaga et al., 2000). The travel time inversions are performed iteratively 20 times updating the model with the result of previous inversions at each iteration resulting in better models at each iteration (Korenaga et al., 2000). To stabilize the inversion and save computing resources, 1-D smoothing constraints are applied to both the horizontal and vertical directions independently (Korenaga et al., 2000). We used smoothing and damping parameters ranging from ~6-16 (figure 8). The smoothing parameter was chosen by performing inversions on our 1-D model (figure 6a) with changing smoothing parameters from 1 to 50 incrementing by 0.1. Final models were analyzed based on how large of a change (if any) occurred from the original model, and how reasonable

that change is. Changing final model outcomes from an initial 1-D model with varying smoothing parameters can be seen in figure 8. The damping parameter, which controls the level of percent velocity change, was chosen by using the lowest value possible that would result in a stable inversion.

Understanding the size of structures that can be recovered in velocity models is critical for accurate interpretation. To test the resolution of our models we perform checkerboard tests with three varying sizes of anomalies (figure 9). The size of the anomalies added are 60mx10m, 100mx10m, and 200mx30m. We do these tests by taking the preferred starting model (figure 6b) and adding ±0.3km/s in alternating layers forming a checkerboard pattern. We then create synthetic data from the checkerboard model. Lastly, we invert the original model with no anomalies and observe how well our final model can recover the anomalies. The results from this process are shown in figure 9. From our checkerboard tests we appear to be recovering the horizontal locations of the anomalies well, but the vertical extents are not recovered. The minimum size of a structure that we can resolve horizontally appears to be about 80m (figure 9). This means that we have better horizontal resolution compared to vertical resolution which seems to agree with our inversion results from figure 6 where we do not see many vertical structures mainly just horizontal structures.

Calculating H/V Spectral Ratios Workflow

We explore what information can be gained about the subsurface from H/V spectral ratio calculations in a shallow hydrothermal setting. The H/V ratio is the ratio of the Fourier amplitude spectra of the horizontal to the vertical component of the seismic recording. H/V ratios highlight potential amplifications in Rayleigh waves due to discontinuities and can be useful for determining the level of relative compaction and rigidity of the underlying lithology (Nakamura,

2008). Generally, the higher the H/V ratio, the less rigid the subsurface is relative to the surrounding area (Nakamura, 2008). Variations in the H/V ratio over time may indicate fluid movement because the horizontal component is relatively stable regardless of the presence of fluids, but the vertical component will increase with fluids present (Lontsi et al., 2019). H/V analysis is a good addition to our tomographic models and provides information over a broader spatial area than our 2-D profiles. Furthermore, H/V analysis allows for temporal monitoring as well.

The H/V ratio method is highly dependent upon select frequency ranges and is typically used to determine the resonant frequencies at locations for site effects studies (Rincon et al., 2016). However, in this study we explore the broadband H/V ratio over a time window before and after OFG eruptions. In future work we will calculate the resonant frequencies at each station to better understand how the frequency dependence changes spatially across our array.

We calculate two North-South East-West arrays and the full 3-D array for H/V ratio values for a time window of 90 minutes relative to the time of the eruption. We calculate the H/V ratios for 60 minutes before the eruption and 30 minutes after the eruption. An example of the raw data recorded on station 553 over this 90-minute time interval is shown in figure 10. A sliding time window of 20s with an increment of 1s is used to calculate the H/V spectral ratio. The eruption times came from the website 'geysertimes.org'. Our two East-West and North-South arrays were deployed on 11/09/2016 and 11/11/2016. We chose these arrays because the array deployed on 11/09/2016 crosses the OFG orifice and the array deployed on 11/11/2016 crosses the proposed reservoir location. The locations of stations used for these two lines are shown in figures 11 & 12. The full 3-D array is utilized by averaging the H/V ratio values for the 90-minute interval around the eruption over each station on each day. Then, once the H/V

ratio values have been calculated for each station on multiple days we took the average of the H/V ratios over the 90-minute time window for each station. Finally, we extract H/V ratios for 4 unique times relative to the eruption: -55, -25, 5, & 20 minutes where negative time indicates it is before the eruption. We use the H/V ratio at these time values to create a 2-D contour plot of the H/V ratio values changing with time (figure 13). Examining the H/V ratio in 1-D and 2-D provides insight into what kind of information we can gain from this method at an active hydrothermal field.

Results

Our results show features which provide insight into the hydrothermal plumbing system beneath OFG. The active source seismic refraction study allows us to visualize velocity changes in the upper ~50m of the subsurface based on the ray penetration (figure 6). We supplement the tomographic profiles with H/V ratio calculations which give us insight into subsurface rigidity which could correspond to zones of saturation (Nakamura. 2008). The velocity profiles we generate may be useful for determining horizontal extent of subsurface structures.

Tomographic Profiles

Generating tomographic P-wave velocity profiles in media that is highly attenuating is challenging due to the limited ray coverage over the whole model. This makes the inversion process unstable (Aster et al., 2013). Due to this challenge it is important to utilize as much prior geologic knowledge about the region as possible in order to get the inversions to converge to a final model. We tried many different initial velocity models, but present only two initial velocity models here based on previous geologic models (figure 6b), and a 1-D velocity gradient with velocity increasing as a function of depth (figure 6a) (Fenner., 1936; Foley et al., 2014; Muffler et al., 1982; Wu et al., 2017). The velocity model based on previous research (figure 6b) was

created with two velocity zones increasing with depth and grading into one another. Model 6b was designed to model the generalized cross sections presented by Wu et al. (2017) and Foley et al. (2014). Figure 6 shows the initial and final velocity profiles for the models. The 1-D gradient model converges to something that is similar in structure to the other model but has significantly different velocities.

The velocity profiles in figure 6a & 6c show the starting and final profile made with the 1-D velocity gradient. This model was made with a V_p on the surface of ~2.8km/s increasing at regular intervals to 100m below the surface with a V_p of ~4.5km/s. The final model has good ray coverage NE of the OFG orifice to depths of ~50m below the surface. The ray coverage SW of the OFG orifice is fair, but only penetrates ~20-25m below the surface. We observe one interesting velocity discontinuity in this final model which we will refer to as 'Q' (figure 6c). Velocity discontinuity 'Q' begins ~150m SW of OFG where our stations are present and extends laterally ~140m. The narrow zone of decreased velocity lowers the velocity gradient from the area to the SW ~10m vertically. This zone has roughly a 20% velocity reduction compared to the surrounding area. Aside from this low velocity zone we do not observe any other significant changes from the background model aside from the velocities decreasing from the initial model.

The next profile we will consider is the one shown in figure 6b & 6d. This tomographic profile has higher velocities in the NE and lower velocities in the SW to model the transition from rhyolites to glacial deposits. This inversion was done with a smoothing parameter of 5 and a damping parameter of 15. These parameters were chosen because they gave the model enough 'freedom' to change but did not allow it to change to an unreasonable extent. After the inversion process was performed we see a slight velocity pullup near a transition from lower to higher velocities. This pullup is beneath the label 'R' in figure 6d. This pullup could mark the transition

from glacial deposits to rhyolites. From our resolution tests (figure 9), we should be able to resolve a lateral transition zone such as this. In the final model we observe the average velocity where we expect glacial deposits to be around 1.5-1.8km/s. In the rhyolite units the velocity ranges from ~2.2-3.8km/s. Again, in this model, ray coverage is more robust with deeper penetration in the NE than it is in the SW. We recover another interesting velocity structure labeled 'Q' on figure 6d. The 'Q' anomaly is located ~150m SW of OFG and extends ~280 SW of OFG which is roughly the same location as 'Q' in figure 6c. This anomaly has a velocity ranging from ~1.15-1.4km/s and has good ray coverage in the region that the anomaly is present. This anomaly has a ~25% velocity reduction compared to the surrounding area and a ~50% velocity reduction compared to the rhyolites in the NE. The model shown in figure 6d is our preferred final velocity model because it has good ray coverage throughout the model and seems to be the most realistic when compared to previous studies (Foley et al., 2014, Wu et al., 2017). The RMS error of this model is 0.04 seconds.

H/V Ratio Calculations

We calculated the H/V ratio at stations crossing N-S and E-W of the OFG orifice and stations crossing N-S and E-W ~150m SW of OFG (figures 11 and 12). Calculations were done over an interval of 90 minutes around the eruption of OFG. Calculations were done using a sliding window of 20s which incremented by 1 second each iteration.

The H/V calculations done on the N-S & E-W arrays crossing the OFG orifice are shown in figure 11. On the line trending N-S we observe a trend where the H/V ratio is generally lower closer to OFG. Stations 552, 553, 556, 557, & 555 show a decrease in H/V ratio values immediately following the eruption whereas station 554 shows an increase immediately after the eruption. Stations 552, 553, 554, & 556 return to their pre-eruption H/V values 3-5 minutes after

the eruption. Stations 557 & 555 rise to higher H/V ratios than before the eruption 3-5 minutes after the eruption before falling to relatively low values ~15 minutes after the eruption then rising again to a relatively constant value (figure 11). On the line trending E-W we observe station 548 rise in H/V ratio value ~1 minute before the eruption and decrease ~1 minute after the eruption whereas stations 568 & 583 show the opposite behavior. Stations 548, 568, 554, & 555 show an increase in H/V ratio until ~35 minutes before the eruption before decreasing until the eruption. It is notable that these are the four closest stations to the OFG orifice (figure 11a). The other stations on the E-W line also show that the H/V ratio is lower closer to the OFG orifice. Observing H/V ratios on lines crossing over the OFG orifice give us a rough idea of how the lithological properties may be changing in the subsurface.

Our N-S E-W array shown in figure 12a crosses ~170m SW of OFG which is roughly on top of the proposed reservoir location (Wu et al., 2017). The stations used were recording on 11/11/2016 and the H/V ratio calculations are shown in figure 12. The N-S line shows that stations closer to the center of the line display a higher H/V ratio than those further North or South. On the E-W line we observe no distinguishable pattern for the stations before the eruption regarding their location from East to West. Stations 001, 325, 331, & 312 all show a slight drop in H/V ratio value ~16 minutes after the eruption before quickly returning to their average values. It is notable that our stations from the arrays crossing the proposed reservoir location have a higher H/V ratio on average than our stations crossing the OFG orifice (figure 11 & 12).

It is useful to consider the uncertainty in our H/V ratio values. The uncertainty in our H/V ratio calculations was determined by calculating the mean and standard deviation of each of the H/V ratio values at a particular station for each of the 90-minute time windows. On average the standard deviation for the H/V ratio at any station is ~0.06. The maximum standard deviation in

the H/V ratio at any station is ~0.1. Therefore, we are confident that our H/V ratio calculations are accurate within ±0.1.

The results from the H/V ratios calculated for all stations at 2 time intervals before and after the eruption are shown in figure 13. The times that were used for the H/V ratios in figure 13 are: -55, -25, 5, & 20 minutes where negative time indicates it is before the eruption. From this figure we observe only one location, labeled 'S' in figure 13 that shows a significant change over the 4 time intervals. The area labeled 'S' is right on the surface location of the OFG orifice and we observe a decrease in the H/V ratios calculated at this location 5 minutes after the eruption (figure 13c). The other areas which may be significant are labeled 'U', and 'D' in figure 13a & 13c. Both 'U' and 'D' show much lower H/V ratios than the surrounding region. The zones of high and low H/V ratios shown on figure 13 provide insight into the subsurface properties beneath our full seismic array.

Our results from tomographic profile modeling and H/V calculations provide useful insight into the structure of the OFG hydrothermal plumbing system. We can more precisely characterize the lateral extent of the proposed reservoir described by Wu et al. (2017) in the subsurface due to the resolution of P-wave travel time tomography. Furthermore, we are exploring how the H/V ratio technique can be applied to study the subsurface in active geyser fields.

Interpretation & Discussion

Tomographic Profiles

From our 2-D tomographic profiles shown in figure 6 we observe that we are recovering one major low velocity zone and possibly get some information about the subsurface location of the rhyolite-glacial deposit interface. The first anomaly we will consider, labeled 'Q', begins

~150m SW of the OFG orifice where our stations begin SW of OFG and extends laterally from that position ~140m shown in figure 6d. It is unclear whether this low velocity zone extends across the locations in our line where we don't have ray coverage beneath OFG, but it appears that it does since a similar velocity profile is observed where we have stations to the NE. The V_p range in this zone is from 1.15km/s-1.5km/s which is consistent with a highly saturated and porous media. We believe that this zone corresponds to the fractured porous media described by Wu et al. (2017) that acts as a hydrologic reservoir where groundwater and previously erupted waters infiltrate and recharge the OFG plumbing system. Although we cannot constrain the depth of this reservoir we may be constraining the lateral extent to the SW. We observe a 25% V_p reduction between the reservoir and the surrounding area and a 50% V_p reduction between the reservoir and the rhyolites in the northeast which is different than what was reported in previous research where the Rayleigh wave phase velocity reduction was ~70% and ~40% respectively (Wu et al., 2017). The difference in velocity reduction between this study and previous research is likely because we are examining P-wave velocities whereas past research was examining Rayleigh wave phase velocities. We are able to laterally recover the main reservoir on our 2-D profiles, but are not able to recover other structures which have been discovered in source localization research due to the limited ray coverage on our 2-D profile (Vandemeulebrouck et al., 2013; Wu et al., 2019).

The limitations in our ability to constrain the shape of smaller structures which contribute to the OFG plumbing system come from our source and receiver spacings being relatively large at 20-30m, our source not being large enough to propagate across the entire line, and having the ~200m source and receiver gap over the top of OFG. Furthermore, our main target structure (the proposed reservoir ~150m SW of OFG) being a highly fractured surface also plays a role in

scattering and attenuating active source rays. These issues led to limited ray coverage in 2-D, and our difficulty resolving smaller structures was also likely related to attenuation caused by highly hydrothermally altered sediments, a highly fractured region, and a saturated subsurface. Constraining the lower limit of the reservoir is something we are not able to do with our 2-D tomographic profiles. We are also not able to recover smaller structures like those described by Vandemeulebrouck et al., 2013 and Wu et al., 2019. Since this area is highly hydrothermally altered the attenuation of the rays is high as well (Lynne et al., 2017). However, some of these limitations may be overcome by modelling in 3-D with denser source-station pairs, which is planned for future work.

Another interesting structure observed on our 2-D line is located at the rhyolite-glacial deposits interface near the Firehole river labeled ‘R’ in figure 6d. We observe a velocity pull up near the rhyolite-glacial sand interface. Since we are getting good lateral resolution (figure 9) this pull up may mark the transition location from glacial deposits to rhyolites meaning that the boundary is located directly beneath the Firehole River.

In figure 14 we overlay the results from our preferred final tomographic model (figure 6d) with the generalized geologic cross section presented by Wu et al. (2017) which shows the proposed reservoir location. This overlay shows that we may be recovering the lateral extent of the top portion of the reservoir to the SW of the geyser. Although we cannot constrain the vertical extent of this reservoir we may be able to constrain the lateral extent with our 2-D tomographic profiles.

The 2-D tomographic profiles created in this study allow us to obtain new information about the OFG plumbing system in the subsurface. Using active source seismic modeling in an active hydrothermal field is a viable method to study the subsurface. Densely spaced, well

coupled seismic arrays with powerful sources are likely needed to do reflection imaging in hydrothermal areas. However, P-wave refraction tomography can be done with less powerful sources and lower coupling to get useful velocity profiles. Our 2-D tomographic profiles created in this study furthers our understanding of the OFG hydrothermal plumbing system.

H/V Ratio Calculations

H/V ratio calculations of a seismic signal can lend insight into the relative rigidity of the subsurface (Nakamura, 2008). A more rigid subsurface will have amplitudes that are similar in the horizontal and vertical directions whereas less rigid subsurface lithologies will have greater amplitudes in the horizontal direction (Nakamura, 2008). Therefore, where H/V ratios are higher the subsurface is assumed to be less rigid (Nakamura., 2008). We may also be able to detect fluid movement using the H/V ratio since the horizontal component is generally unaffected by fluids and the vertical component will increase with fluid saturation (Lontsi et al., 2019).

We will begin by examining the H/V ratios calculated for the stations shown in figure 11 which cross the OFG orifice. The four stations closest to the OFG orifice (548, 568, 554, & 555) show an increase in H/V ratio until ~35 minutes before the eruption before decreasing until the eruption. This pattern may correspond to fluids moving into reservoirs beneath the geyser making the subsurface more rigid than migrating closer to the orifice and causing the surrounding area to lose rigidity. Stations 556, 554, 552, 553, 583, 555, 557, & 568 show decreases in H/V ratio just as the geyser erupts which corresponds to the evacuation of fluids in the subsurface since the vertical component becomes more dominant without fluids present (Lontsi et al., 2019).

We will now examine the H/V ratios calculated for the stations shown on figure 12 which were recording on 11/11/2016. The stations shown in figure 12 cross the proposed reservoir

location in the N-S & E-W directions over the proposed reservoir location. These stations have a higher H/V ratio on average than the stations shown in figure 11. This could mean that the subsurface lithology around the proposed reservoir location is more rigid than the subsurface surrounding the OFG orifice. Stations 001, 325, 331, & 332 all show a slight drop in H/V ratio value ~16 minutes after the eruption before quickly returning to their previous values. This sudden drop could be from local fluid movement or local bubble collapse. The broadband H/V ratio values appear to only have significant variations after an eruption which is a dramatic fluid movement over a short period of time. Examining the frequency dependence of the H/V ratio in future work should provide more insight into the properties of the subsurface.

The plots in figure 13 show the H/V ratio values for each station at 2 time intervals before and after the eruption. We observe a few zones of lower H/V ratio than the surrounding areas, labeled 'S', 'U', and 'D' in figure 13. These zones of low H/V ratio indicate that there is likely a higher relative rigidity in the subsurface than the surrounding areas. Zone 'U' is close to the proposed reservoir location (figure 13a). The high H/V ratio values in this area may mean that the reservoir is more rigid than the surrounding region. Zone 'S' is surrounding the OFG orifice and decreases in H/V ratio significantly 5 minutes after the eruption (figure 13c). This signature may be due to the evacuation of fluids causing the vertical component to become more dominant (Lontsi et al., 2019). Zone 'D' is a single station with relatively few stations surrounding it (figure 13e) which could mean this area of low H/V is an outlier in the data.

Conclusion

Utilizing both seismic refraction tomography and the H/V method to characterize the plumbing system of Old Faithful Geyser (OFG) is an effective approach to studying the OFG system. Our 2-D tomographic profiles provided new insight into how P-wave velocities vary

throughout the system. This has helped us constrain the lateral extent of what is believed to be a reservoir body feeding the OFG eruptive cycles. In future work we aim to improve upon the tomographic profiles shown here by utilizing the full 3-D seismic survey and creating tomographic models in 3-D. This should help us to constrain the upper and lower limits on the size of the reservoir we have recovered in the 2-D profiles with greater ray density around the proposed reservoir location. The H/V method is more ambiguous than tomographic modeling but provides meaningful insight into how the subsurface is changing over time before an eruption. By using the H/V method we were able to see which stations are more rigid than the surrounding area and which stations are most heavily affected by fluid movements. In future work with the H/V method we will analyze the frequency dependence of each station. Using both seismic refraction and the H/V method we understand the subsurface plumbing system related to OFG in greater detail than by using either method on its own.

List of Figures

Figure 1: Location of Study Area.

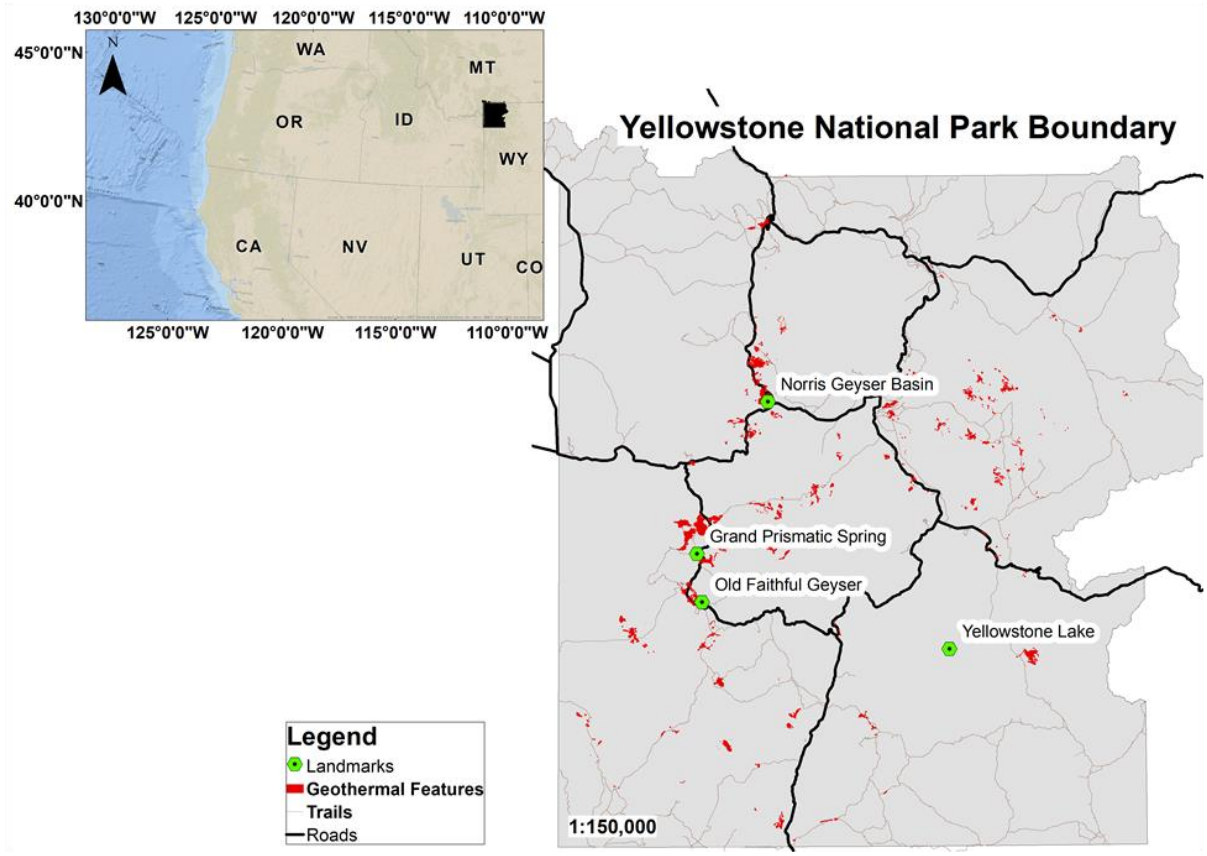

Figure 1 Shows the geographic location of our study area located in NW Wyoming, USA inside Yellowstone National Park. The study area is in Yellowstone National Park near Old Faithful Geyser.

Figure 2: Seismic Array and Geologic Map.

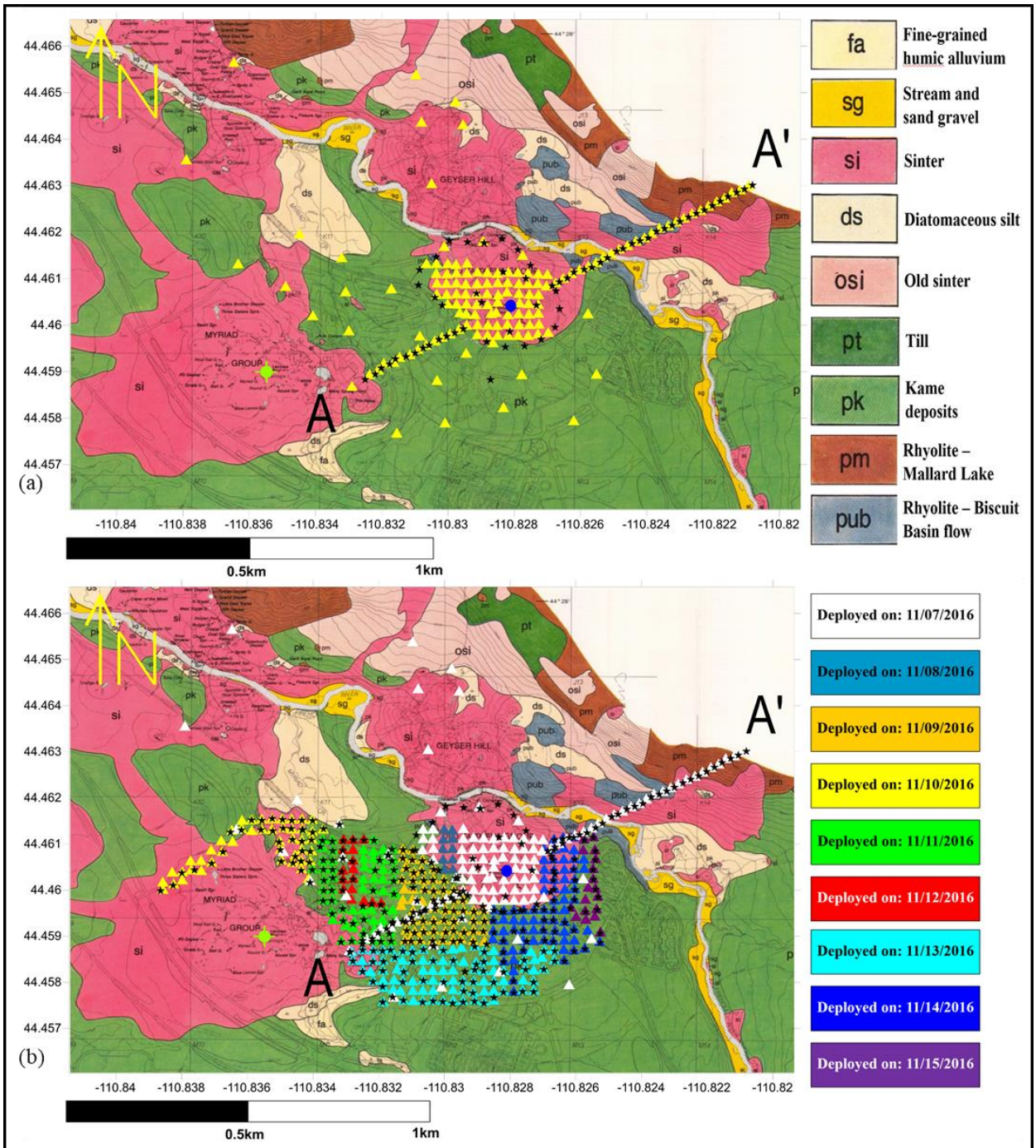

Figure 2 Shows the seismic grid setup, and the locations of Old Faithful Geyser and the C-1 drill hole overlain on a geologic map adapted from Muffler et al., 1982. The yellow triangles in (a) represent our receivers, black stars represent shot locations, the blue circle is Old Faithful Geyser, and the green drill hole symbol is the C-1 drill hole. The deployment shown in (a) was done on 11/08/2016 and is used for our 2-D tomographic profiles. (b) shows 3-D seismic array color coded based on the day they were first deployed. Note that in (b) many stations deployed on previous days are overlapped by those deployed on subsequent days.

Figure 3: Synthesis of Previous Research.

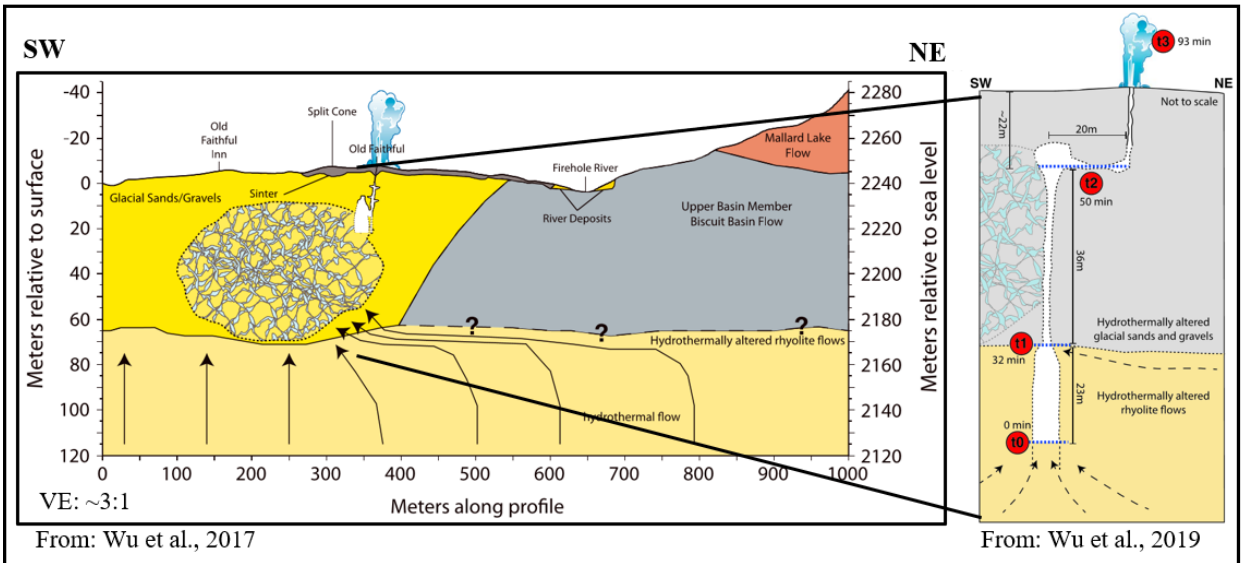

Figure 3 Shows the current model describing the OFG plumbing system presented by Wu et al., 2017, and Wu et al., 2019. It is noteworthy that the uppermost ~20m of the model presented by Wu et al., 2019 had built upon the work presented by Vandemuelebrook et al., 2013 by investigating the source localization deeper.

Figure 4: Example of Shot Gathers.

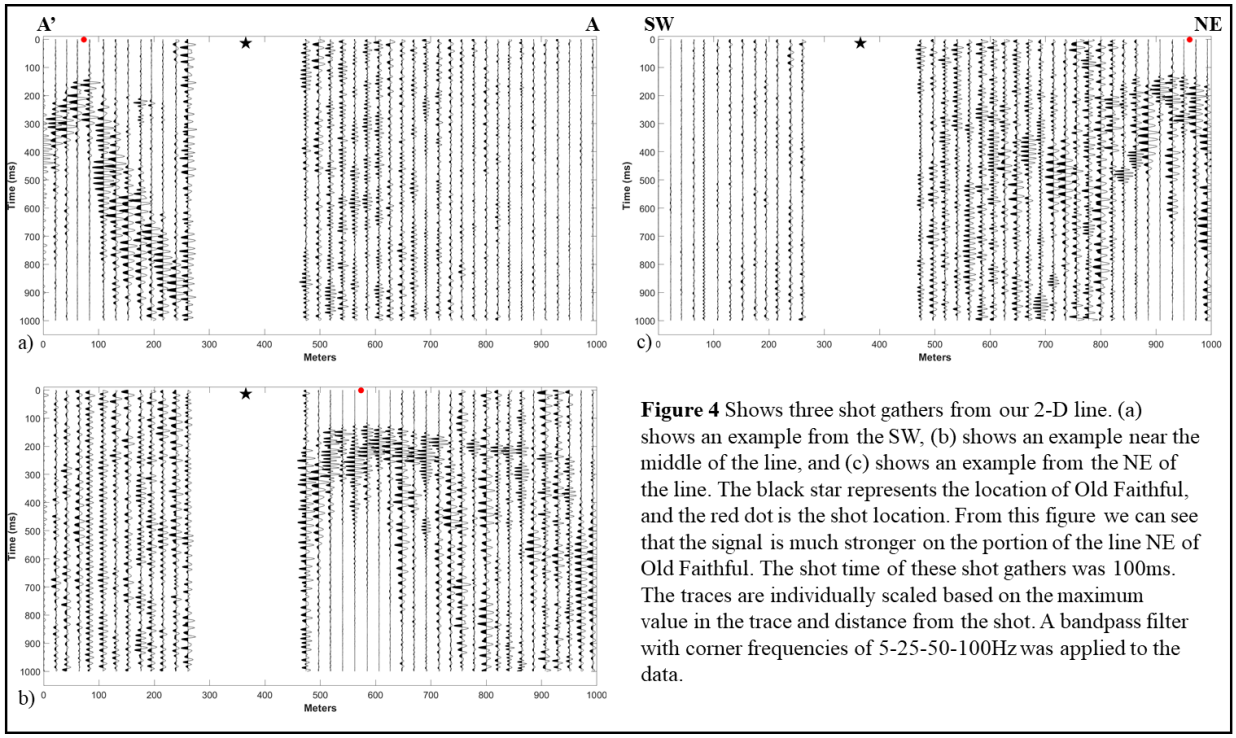

Figure 4 Shows three shot gathers from our 2-D line. (a) shows an example from the SW, (b) shows an example near the middle of the line, and (c) shows an example from the NE of the line. The black star represents the location of Old Faithful, and the red dot is the shot location. From this figure we can see that the signal is much stronger on the portion of the line NE of Old Faithful. The shot time of these shot gathers was 100ms. The traces are individually scaled based on the maximum value in the trace and distance from the shot. A bandpass filter with corner frequencies of 5-25-50-100Hz was applied to the data.

Figure 5: Picks Along 2-D Line.

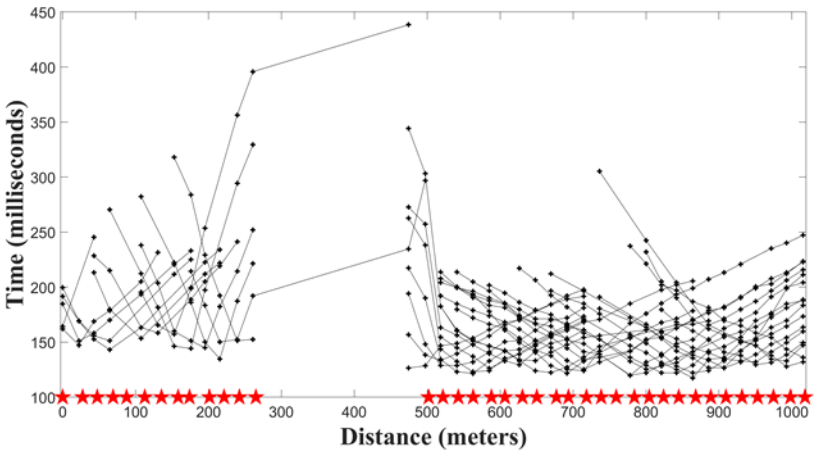

Figure 5 Shows the first arriving P-waves picked along our 2-D line from a Z-component shot record. Red Stars mark the locations of shots. The black dots show the first arriving P-wave picked at each station.

Figure 6: Tomographic Models.

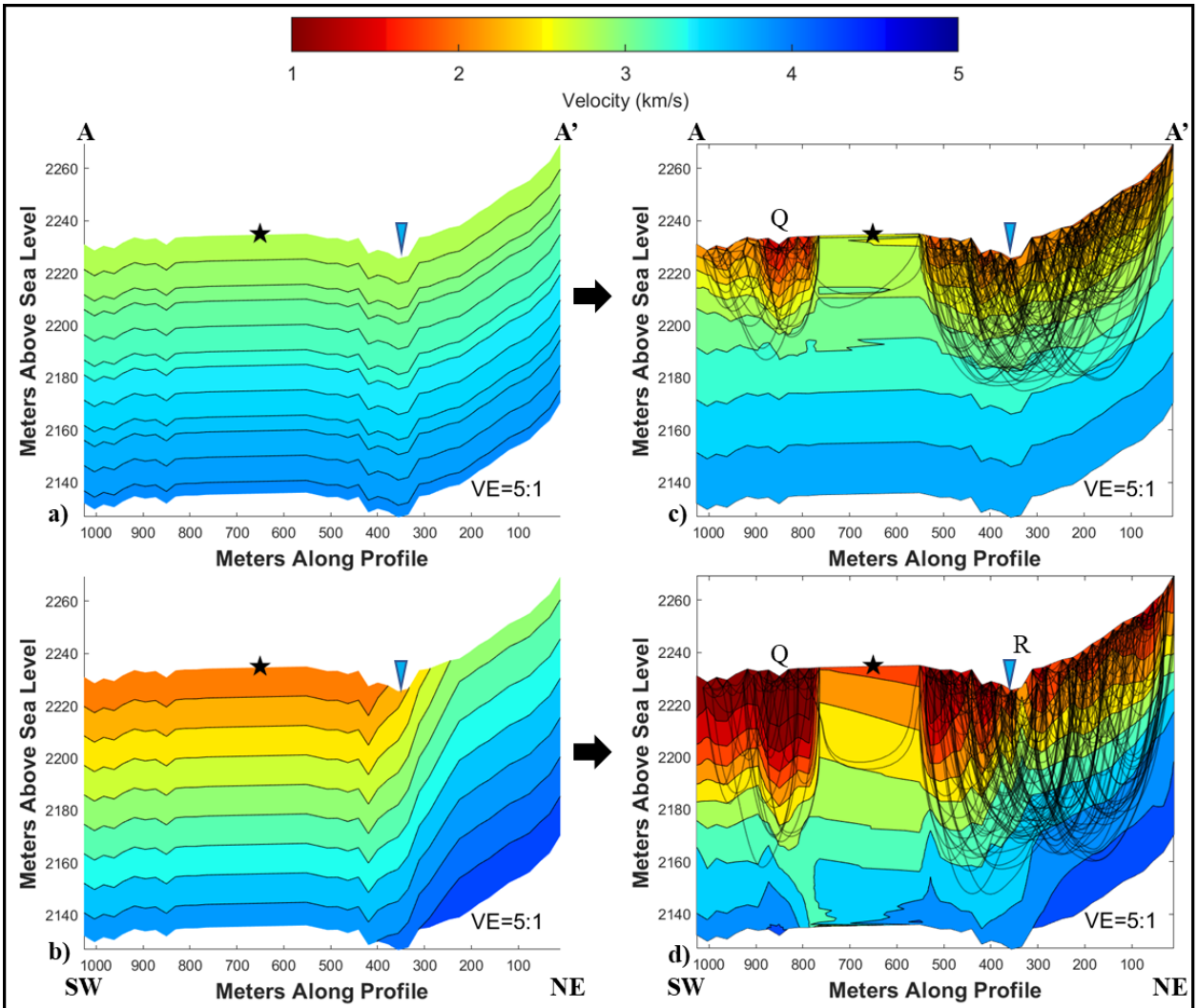

Figure 6 Shows starting (a & b) and final (c & d) models obtained after 2-D tomographic inversions. The black star represents the surface location of the OFG orifice, and the blue triangle is the location of the Firehole River. The areas labeled 'Q' & 'R' are done so to mark the locations of velocity contrasts which are discussed.

Figure 7: Velocity Mesh Setup.

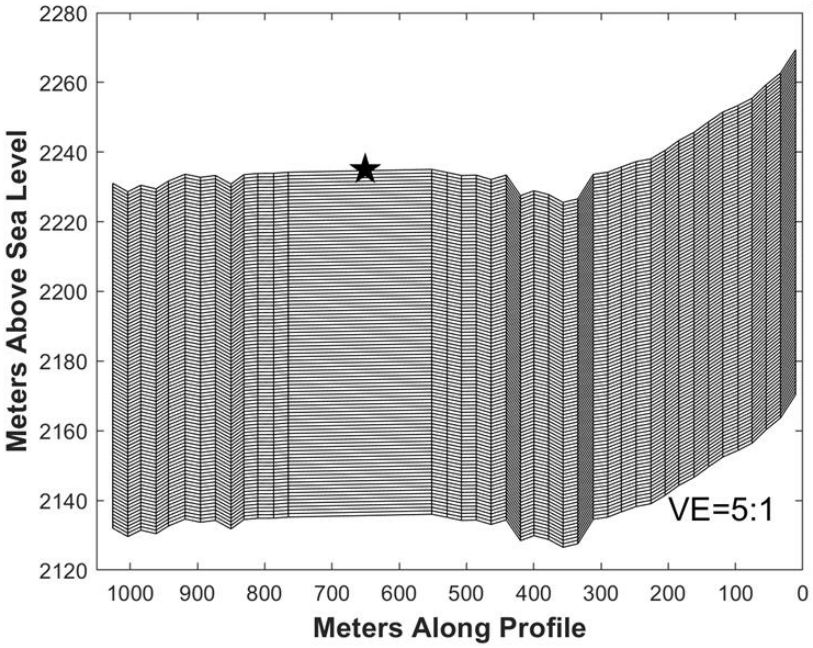

Figure 7 Shows the velocity mesh that was used in our travel time inversions. The velocity nodes are located at the intersections of lines. The black star represents the location of the Old Faithful Geyser orifice.

Figure 8: Smoothing Parameters.

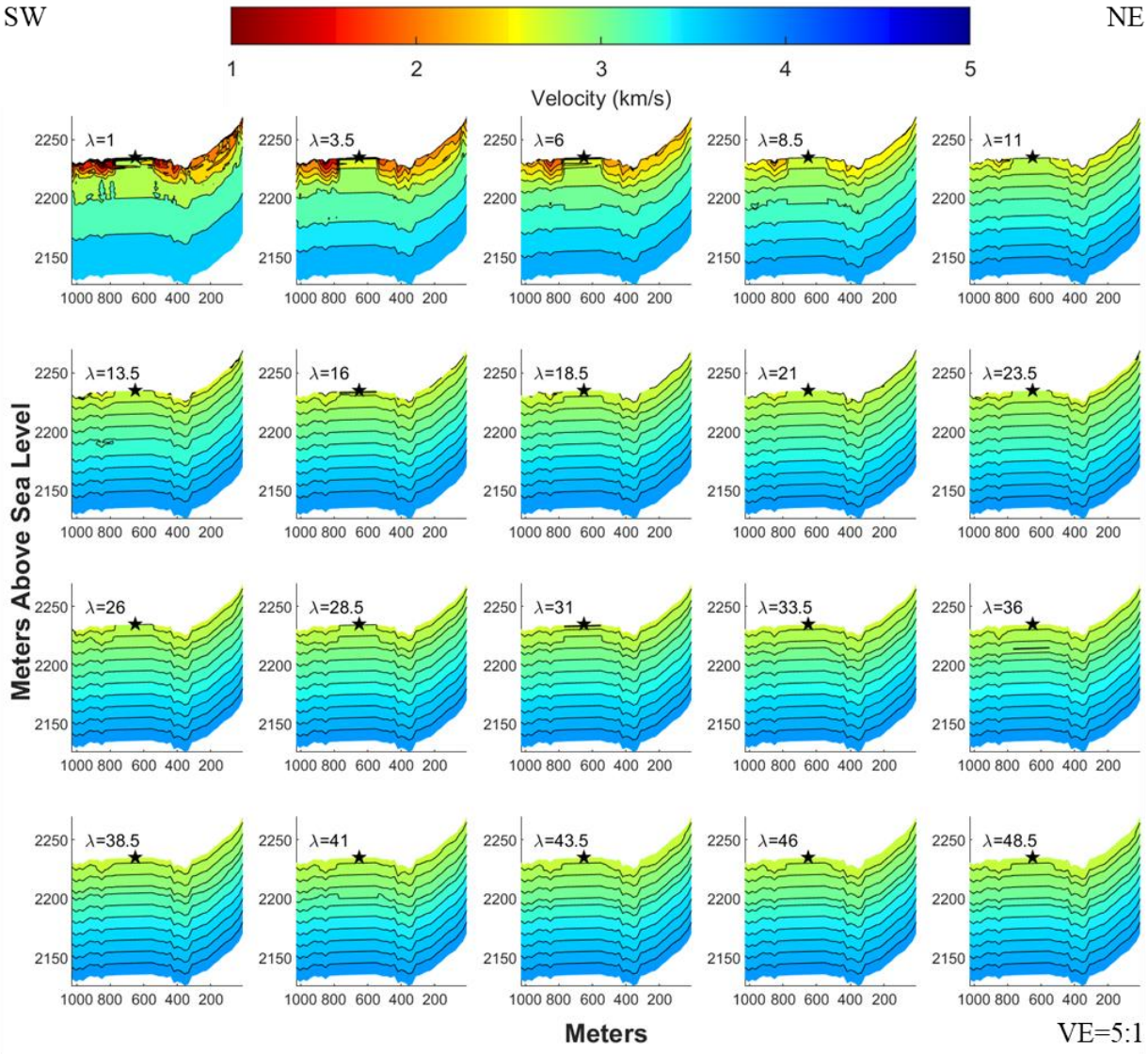

Figure 8 Shows the results of the final model solution with varying smoothing parameters. We see that the best range for the smoothing parameters is ~6-16. The starting model for each of these inversions is the starting model shown in figure 6a. Lambda represents the smoothing parameter in each respective model.

Figure 9: Resolution Tests.

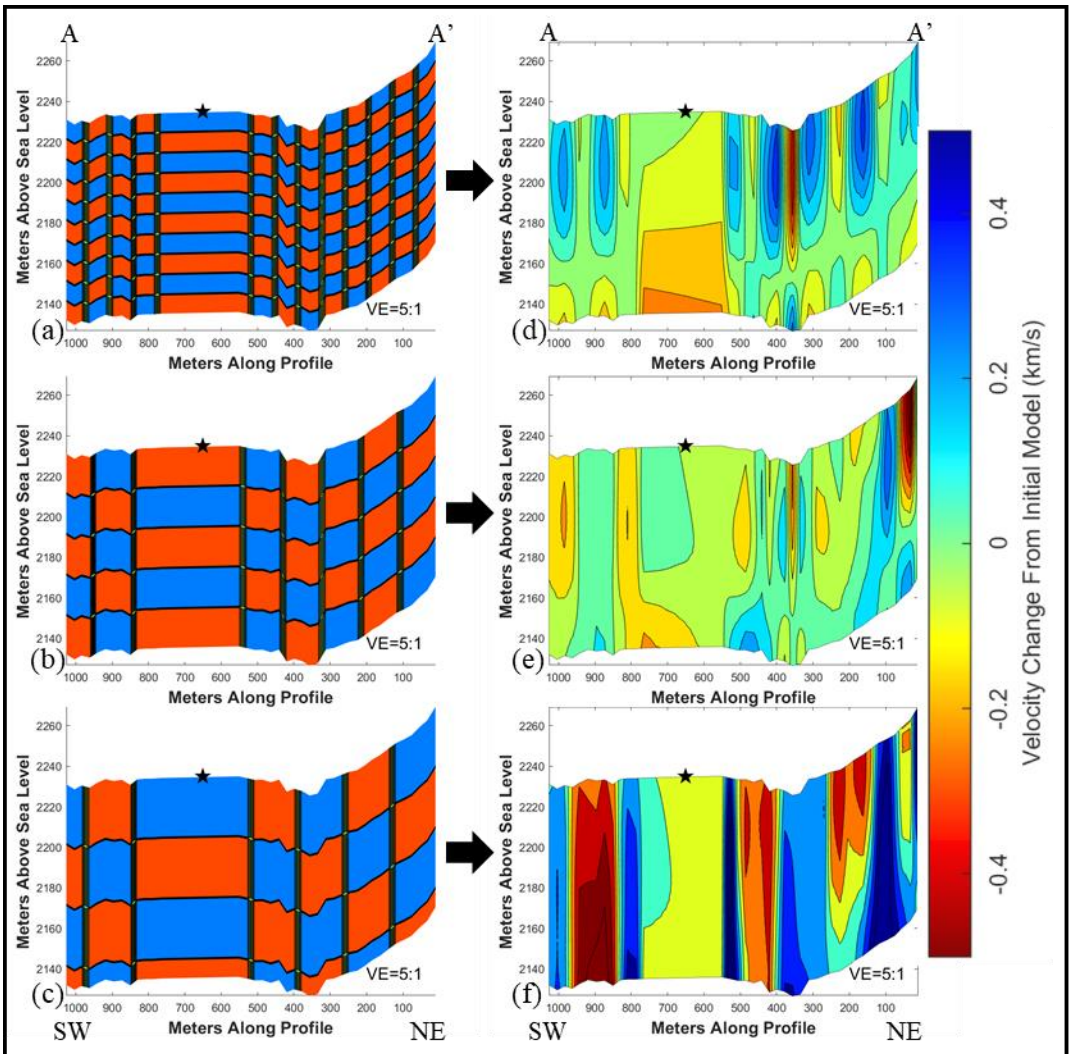

Figure 9 Shows the results of our checkerboard tests. The 1-D gradient model used to add checkerboard anomalies is shown in figure 6a. The anomalies added to the original 1-D model increase in size from (a) to (b) to (c). (d), (e), & (f) shows the checkerboard recovered after the inversion. From this figure we see that we have much better horizontal resolution compared to vertical. The black star represents the location of the Old Faithful Geyser orifice.

Figure 10: Raw Seismogram of Data Recorded over 90-minute Interval Used for H/V Calculations.

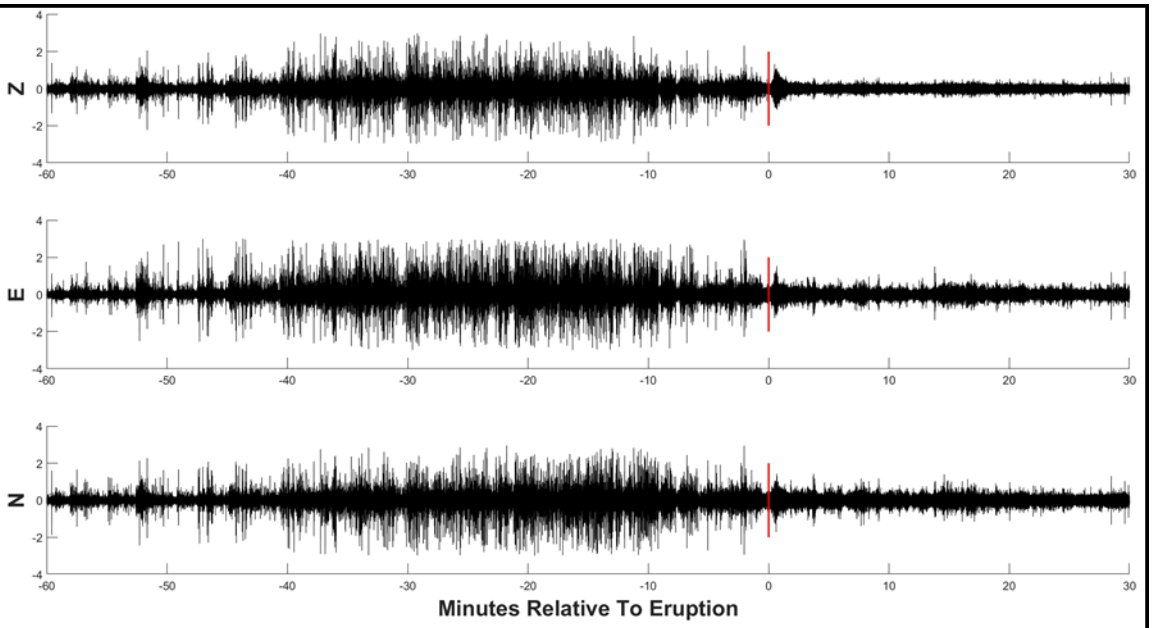

Figure 10 shows the seismic signal from station 553 over the time interval that is used to compute the H/V ratios shown in figures 11 & 12. This eruption took place on 11/092016 at ~8:30am. The x-axis is relative to the eruption of OFG where negative time indicates time before the eruption. The red line at time 0 marks the eruption.

Figure 11: H/V Ratio Calculations for Stations Recorded on 11/09/2016.

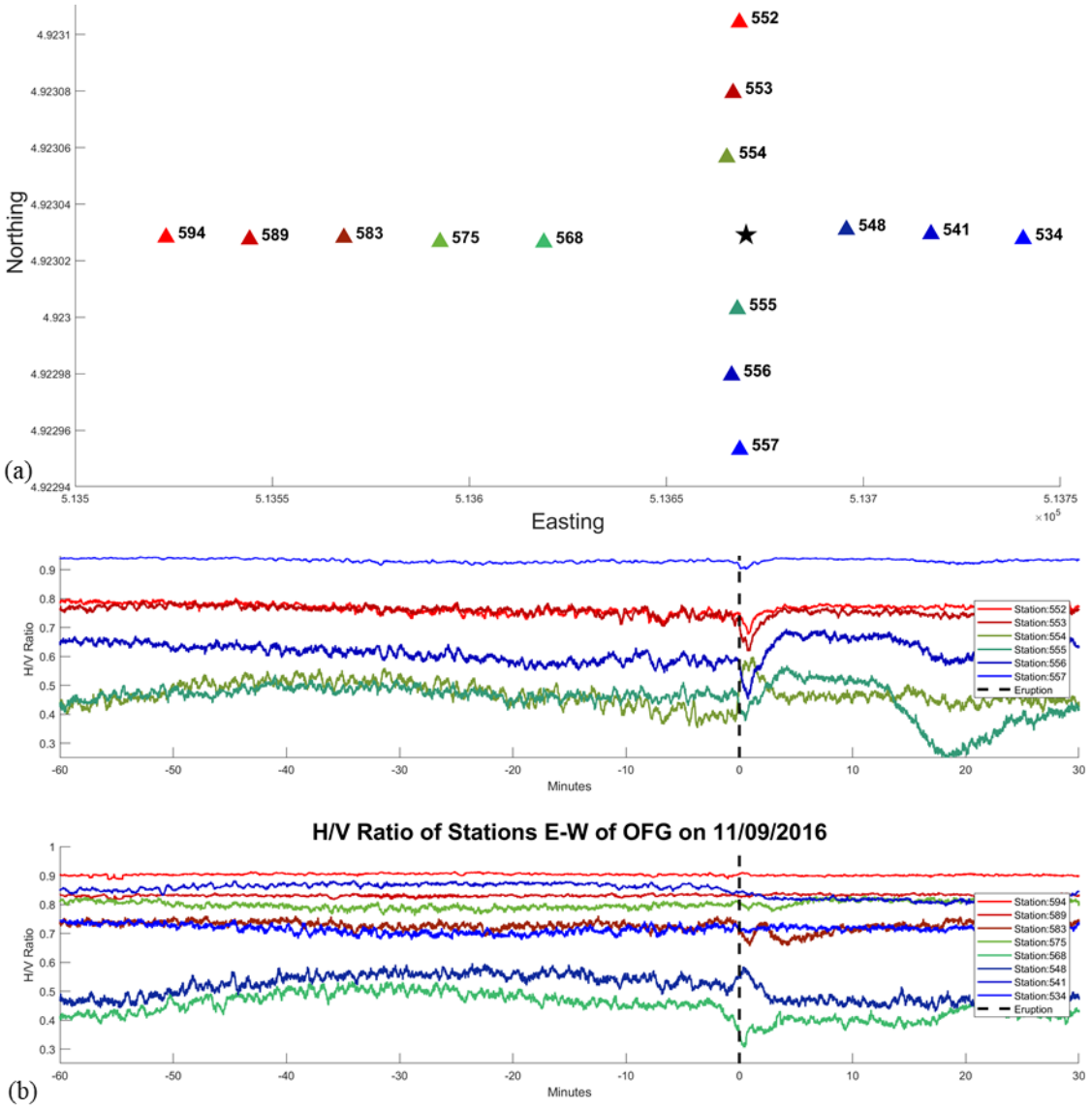

Figure 11 Shows (a) map of station locations used for H/V calculations and (b) H/V calculations done on the N-S and E-W lines crossing over the OFG orifice which were recorded on 11/09/2016. The X-axis in (b) shows time relative to the eruption were negative indicates it is before the eruption. The black star in (a) represents the location of OFG.

Figure 12: H/V Ratio Calculations for Stations Recorded on 11/1/2016.

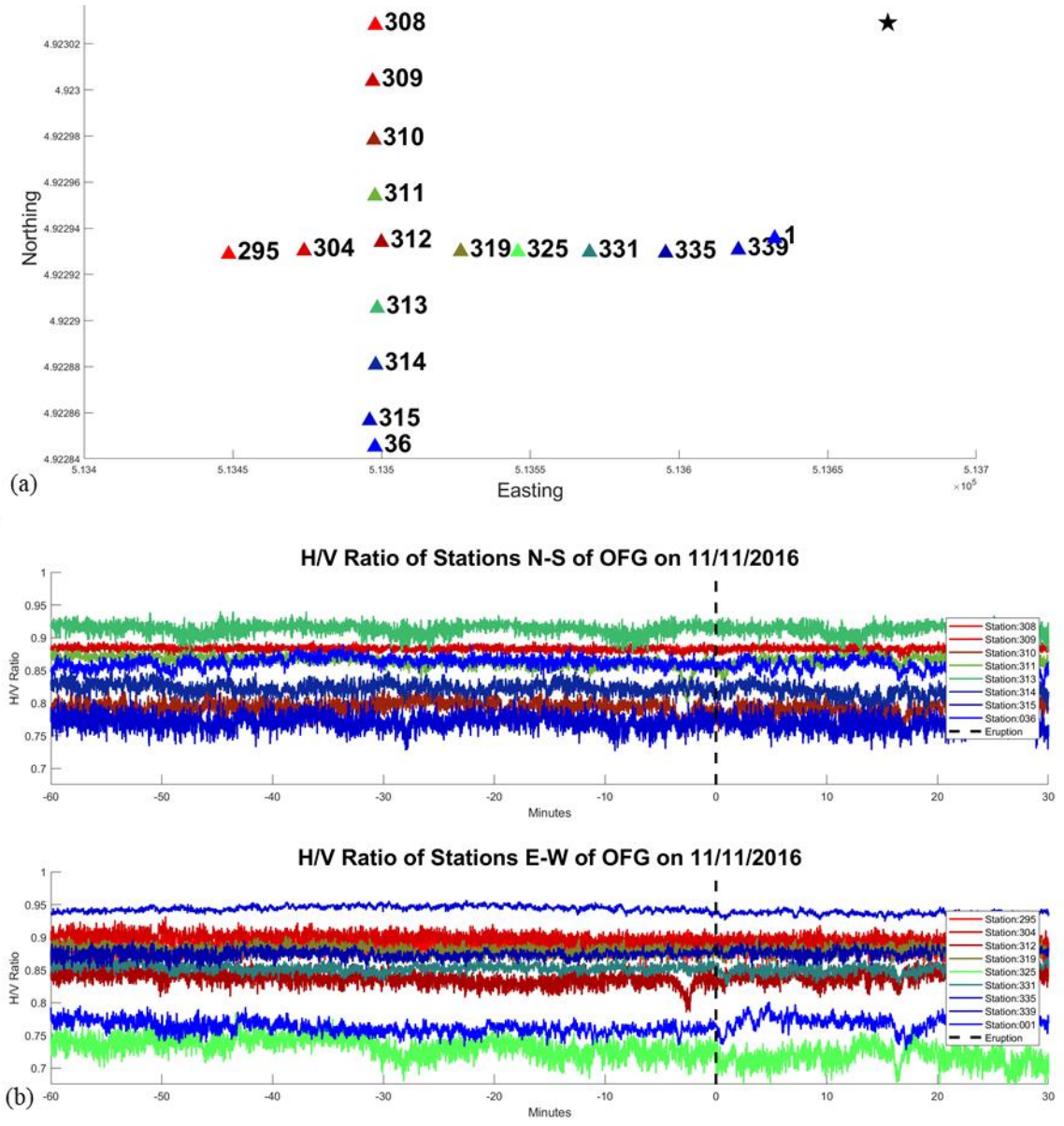

Figure 12 Shows (a) map of station locations used for H/V calculations and (b) H/V calculations done on the N-S and E-W lines crossing over the OFG orifice which were recorded on 11/11/2016. The X-axis in (b) shows time relative to the eruption were negative indicates it is before the eruption. The black star in (a) represents the location of OFG.

Figure 13: H/V Ratios Calculated for all Stations.

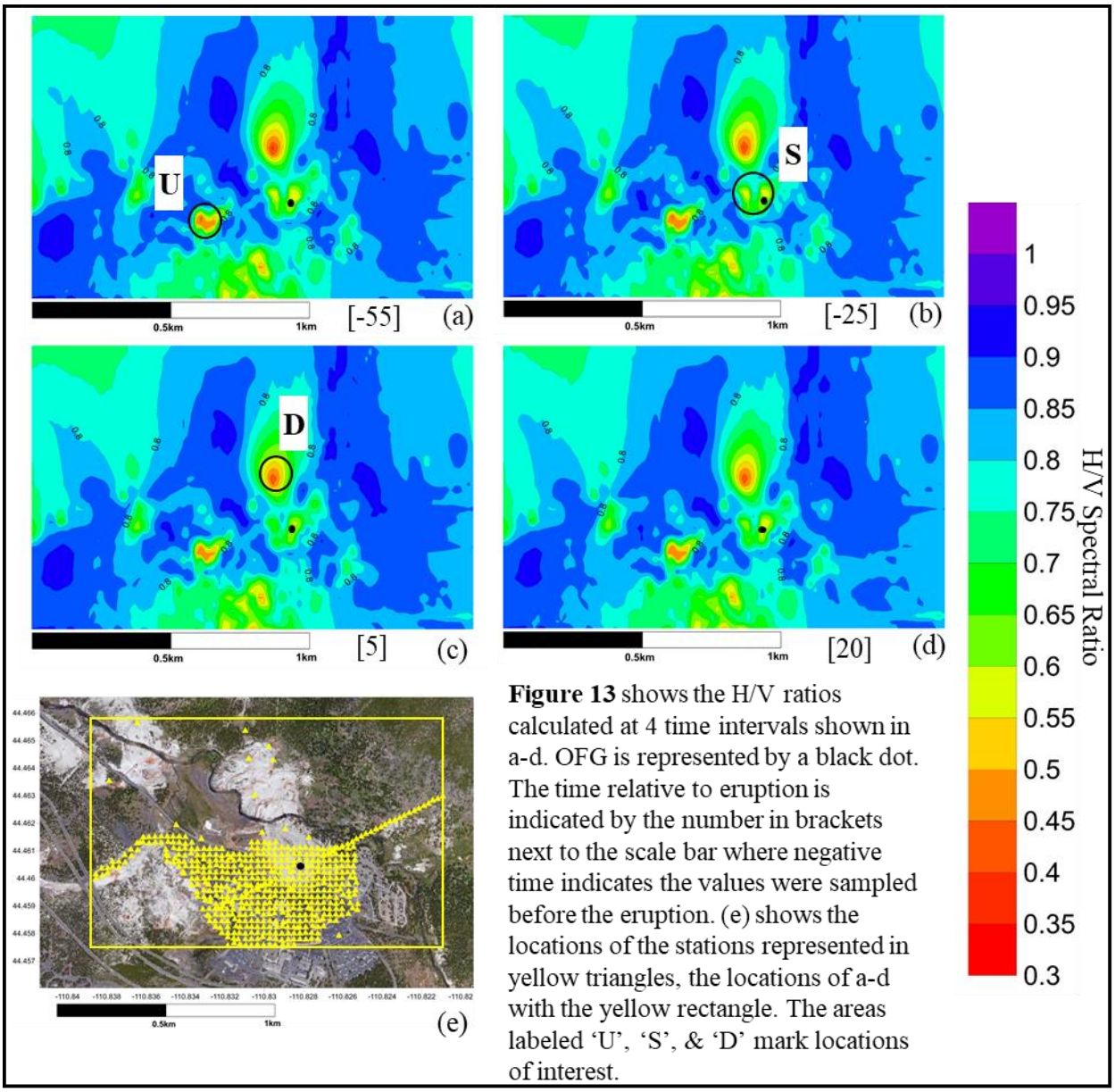

Figure 13 shows the H/V ratios calculated at 4 time intervals shown in a-d. OFG is represented by a black dot. The time relative to eruption is indicated by the number in brackets next to the scale bar where negative time indicates the values were sampled before the eruption. (e) shows the locations of the stations represented in yellow triangles, the locations of a-d with the yellow rectangle. The areas labeled 'U', 'S', & 'D' mark locations of interest.

Figure 14: Overlay of Previous Studies and Preferred Model.

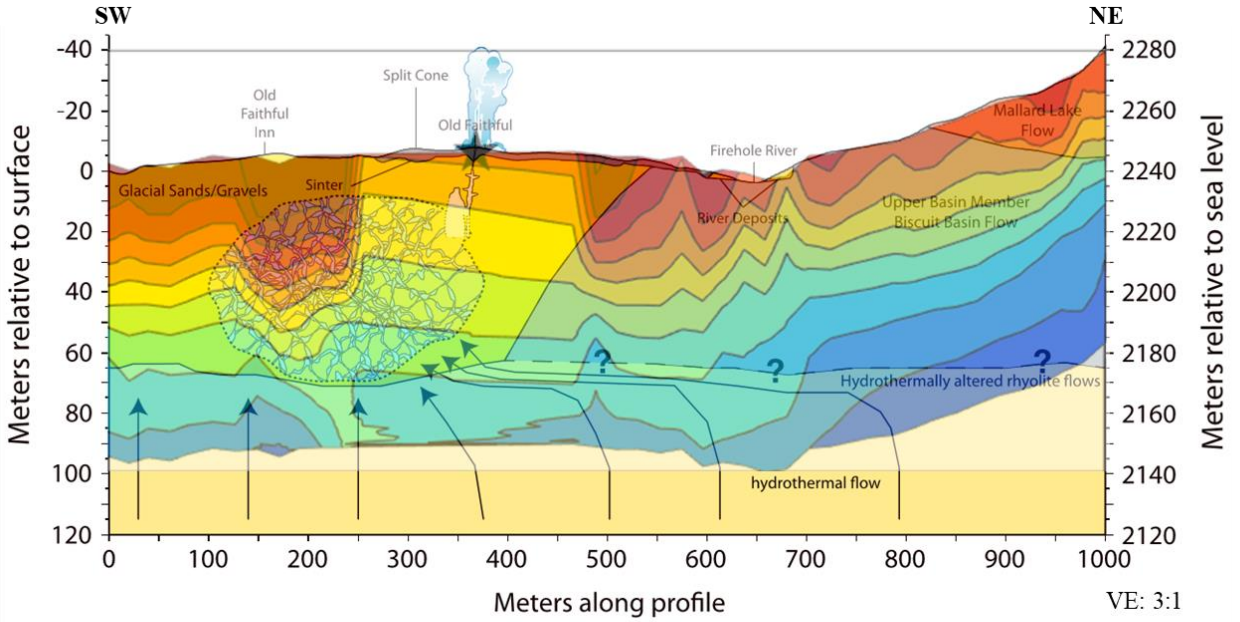

Figure 14 Shows the overlay of our preferred final P-wave velocity model on top of the model presented by Wu et al., (2017). The model we are overlaying with previous results is from figure 6d and has the same color bar. From this image we can see that the low velocity contrast in our model SW of the geyser orifice may partially show the horizontal extent of the reservoir body to the SW of the geyser.

References

Ardid, A., Vera, E., Kelly, C., Manga, M., Munoz-Saez, C., Maksymowicz, A., Ortega-Culaciata, F., 2019, Geometry of Geyser Plumbing Inferred from Ground Deformation, *Journal of Geophysical Research,* 124, 1072-1083.

Aster, R.C., Borchers, B., Thurber, C.H., 2013, *Parameter Estimation and Inverse Problems*, Waltham, MA, Elsevier Inc.

Blackwood, K.W., Sanders, L.A., Gantt-Blackwood, S.I., 2018, Interpreting the origin and evolution of 'karst' features from a siliceous hydrothermal terrane: A case study from the Upper Geyser Basin in Yellowstone National Park, USA, *International Journal of Speleology*, 47, 323-331.

Farrell, J., Smith, R.B., Husen, S., and Diehl, T., 2014, Tomography from 26 years of seismicity revealing that the spatial extent of the Yellowstone crustal magma reservoir extends well beyond the Yellowstone caldera, *Geophys. Res. Lett.*, 41.

Fenner, C.N., 1936, Bore-Hole Investigations in Yellowstone National Park, *The Journal of Geology,* 44, 2, 225-315.

Foley, D., Fournier, R.O., Heasler, H.P., Ingebritsen, S.E., Lowestern, J.B., Susong, D.D., 2014, Hydrogeology of the Old Faithful Area, Yellowstone National Park, Wyoming, and its Relevance to Natural Resources and Infrastructure, Old Faithful Science Review Panel, U.S. Geological Survey Open-File Report 2014-1058, 28 p., http://dx.doi.org/10.3133/ofr20141058.

GeyserTimes (2020), Eruptions of Old Faithful Geyser 2016 [online database]. Available from http://www.geysertimes.org/archive/

Honda, S., Muffler, L.J.P., 1970, Hydrothermal Alteration in Core From Research Drill Hole Y-1, Upper Geyser Basin, Yellowstone National Park, Wyoming, *The American Mineralogist,* 55, 1714-1737.

Huang, H., Lin, F., Schmandt, B., Farrell, J., Smith, R.B., Tsai, V.C., 2015, The Yellowstone magmatic system from the mantle plume to the upper crust, *Science,* 348, 773-775.

Hurwitz, S., & Lowenstern, J. B., 1997, Dynamics of the Yellowstone hydrothermal system, *Reviews of Geophysics*, 52, 375–411. https://doi. org/10.1002/2014RG000452.

Kedar, S., & Kanamori, H., 1998, Bubble collapse as the source of tremor at Old Faithful Geyser, *Journal of Geophysical Research*, 103, 24,283-24,999

Keith, T.E.C., White, D.E., Beeson, M.H., 1978, Hydrothermal Alteration and Self-Sealing in Y-7 and Y-8 Drill Holes in Northern Part of Upper Geyser Basin, Yellowstone National

Park, Wyoming, *Hydrothermal Studies in Yellowstone National Park,* Geological Survey Professional Paper 1054-A.

Korenaga, J., Holbrook, W.S., Kent, G.M., Kelemen, P.B., Detrick, R.S., Larsen, H., Hopper, J.R., Carlo, M., 2000, Crustal Structure of the southeast Greenland margin from joint refraction and reflection seismic tomography, *Journal of Geophysical Research*, 105, 591-614.

Lontsi, A.M., Garcia-Jerez, A., Camilo Molina-Villegas, J., Jose Sanchez-Sesma, F., Molkenthin, C., Ohrnberger, M., Kruger, F., Wang, R., Fah, D., 2019, A generalized theory for full microtremor horizontal-to-vertical [H/V(z/f)] spectral ratio interpretation in offshore and onshore environments, *Geophysical Journal International*, 218, 1276-1297.

Lynne, B.Y., Heasler, H., Jaworowski, C., Smith, G.J., Smith, I.J., Foley, D., 2018, Ground penetrating radar documents short-term near-surface hydrological changes around Old Faithful Geyser, Yellowstone National Park, USA, *Journal of Volcanology and Geothermal Research*, 354, 1-12.

Lynne, B.Y., Smith, G.J., Heasler, H., Jaworowski, C., Smith, I.J., Foley, D., 2017, Post-depositional Alteration of Siliceous Sinter Near Old Faithful Geyser, Yellowstone National Park, USA, *Geothermal Research Council Transactions*, 41, 1-12.

Muffler, L.J.P., White, D.E., Beeson, M.H., Truesdell, A.H., 1982, Geologic Map of Upper Geyser Basin, Yellowstone National Park, Wyoming, *Department of the Interior, USGS, Miscellaneous Investigations Series, Map 1-1371*.

Nakamura, Y., 2008, On The H/V Spectrum, *The 14th World Conference on Earthquake Engineering*.

Pasquet, S., Holbrook, W.S., Carr, B.J., Sims, K.W.W., 2016, Geophysical imaging of shallow degassing in a Yellowstone hydrothermal system, *Geophysical Research Letters*, 43.

Rincon, O., Shakoor, A., Ocampo, M., 2016, Investigating the reliability of H/V spectral ratio and image entropy for quantifying the degree of disintegration of weak rocks, *Engineering Geology*, 207, 115-128

Smith, R.B., M. Jordan, B. Steinberger, C.M. Puskas, J. Farrell, G.P. Waite, S. Husen, W.L. Chang, and R. O'Connell, 2009, Geodynamics of the Yellowstone hotspot and mantle plume: Seismic and GPS imaging, kinematics, and mantle flow, *J. Volcanol. Geotherm. Res.*, 188.

Vandemeulebrouck, J., Roux, P., Cros, E., 2013, The plumbing of Old Faithful Geyser revealed by hydrothermal tremor, *Geophysical Research Letters,* 40, 1989-1993.

Wu, S., Ward, K.M., Farrell, J., Lin, F., Karplus, M., Smith, R.B., 2017, Anatomy of Old Faithful From Subsurface Seismic Imaging of the Yellowstone Upper Geyser Basin, *Geophysical Research Letters*, 44.

Wu, S., Lin, F., Farrell, J., Allam, A., 2019. Imaging the deep subsurface plumbing of Old Faithful geyser from low-frequency hydrothermal tremor migration, *Geophysical Research Letters,* 46, 7315-7322.

Vita

Jordan R. Caylor received his B.S. in geology with a specialization in geophysics from Southern Illinois University before pursuing his graduate degree(s) at The University of Texas at El Paso. Jordan has worked as an undergraduate research assistant, teaching assistant, and interned at Pacific Northwest National Lab. While not studying or working Jordan spends his time volunteering and pursuing outdoor activities.

Typist: Jordan Rigdon Caylor

Contact Information: jrcaylor@miners.utep.edu